Modeling the rheology of suspensions with high-viscosity solvents: A predictive multiscale approach

Athonu Chatterjee, David R. Heine, Amy L. Rovelstad, and Lung-Ming Wu
Corning Incorporated, Corning, New York 14831, USA
(Received 14 April 2009; revised manuscript received 29 May 2009; published 26 August 2009)

In this paper, a multiscale approach spanning atomistic and mesoscopic regimes to model the rheology of suspensions that have strongly interacting particles in highly viscous solvents is presented. The model suspensions studied here have 65% sucrose solution—a Newtonian fluid with a viscosity of 170 cP at room temperature—as the solvent phase with ceramic particles of sizes on the order of a few μms as the dispersed (solute) phase. A multiscale approach is proposed to quantitatively account for the effect of the properties of constituent materials on the bulk rheology of the suspension apart from the effect of hydrodynamic factors. A dissipative particle dynamics-type particle-based approach is adopted to which material-specific, mesoscopic force fields developed using molecular dynamics are fed. Issues pertaining to the handling of the vast spectrum of time and length scales present and an appropriate Gallilean-invariant thermostat for solvent dynamics are addressed and resolved. Numerical calculations compare reasonably well to experimentally measured viscosities up to reasonably high Peclet numbers ($\sim 10^4$).

DOI: 10.1103/PhysRevE.80.021406 PACS number(s): 82.70.Dd

I. INTRODUCTION

Suspensions with highly viscous solvents and strongly interacting solid particles are ubiquitous in industrial applications. In such suspensions, the solvent phase becomes an efficient carrier of momentum and consequently hydrodynamic interactions become significant in determining the bulk viscosity. Also, electrostatic interactions between the solid particles and between the solid particles and the solvent phase become equally significant leading to a strong material specificity in the rheology. To capture the effect of all these disparate interactions that span several decades of length and time scales [1], a multiscale approach is used.

At the mesoscopic scale, a dissipative particle dynamics (DPD)-type particle-based computational framework [2–4] is used. In this approach, the whole system (solvent and solute particles) is discretized into mesoscopic-sized particles; effective mesoscopic interactions between the particles then govern the dynamics of the system and hence its rheology [1]. Most contemporary numerical works in this area consider the qualitative effect of parameters such as solid loading of the suspension, particle shape, particle size, shear rate, etc. on the macroscopic rheology of suspensions [2,4]. More quantitative numerical formulations that also account for the effect of constituent material properties on bulk rheology do not exist to our knowledge. However, it is well known that the effect of material properties on shear viscosity of ceramic suspensions is strong in systems with strongly interacting solid particles, such as the system studied here. In order to have some predictive capability regarding real suspensions, therefore, one needs to account for the material properties in conjunction with the hydrodynamic effects. Material properties manifest themselves as nonhydrodynamic (electrostatic and dispersion) interactions between the particles of the modeled system. An understanding of the effect of these interactions on the bulk viscosity of the suspension entails capturing the material-specific nature of these interactions. By doing so, one can potentially tailor the viscosity predictably by changing the material constituents. With this being one of the main motivations of this work, Derjaguin-Landau-Verwey-Overbeek (DLVO) theory [5] along with atomistic level molecular-dynamics (MD) calculations were employed to calculate the parameters of the solid-solid interactions. The effective interactions thus calculated are used in the mesoscopic DPD framework.

In suspensions, such as the suspension of μm-sized ceramic particles in a 65% sucrose solution studied here, electrostatic interaction between the solid particles and the solvent phase can have a strong effect on rheology. These interactions are nontrivial and like solid-solid interactions, they bring material sensitivity to the rheology of the suspension. Therefore, they need to be characterized and their effect on rheology needs to be parameterized similarly. In the DPD framework, this interaction manifests as the effective interaction between the DPD fluid (or solvent) particle and the larger solid particle. Unlike solid-solid interaction, however, a DLVO-type generic framework does not exist for this interaction partly due to the fact that the interaction-pair members belong to two different phases. In this work, we introduce a Lennard-Jones (LJ) type interaction between these particles and bring material specificity to it by interpreting the LJ parameters in a mesoscopic sense and calculating the interaction parameters using the basic material properties.

The importance of hydrodynamic effects on the shear rheology of these types of suspensions cannot be overstated [2,3,6]. From the point of view of overall rheology of the suspension, the solvent plays the role of carrying the momentum imparted to it by the motion of the solid particles. At higher viscosities, the hydrodynamic effects and viscous dissipation become more prominent and need to be resolved accurately by the numerical scheme. In this work, the Lowe-Andersen thermostat [7] is implemented to resolve the dynamics of the solvent phase within the framework of suspension rheology. From our experience, the original DPD thermostat [2] is inadequate in sufficiently resolving the

momentum-carrying capacity of highly viscous solvents [4]. This is also noted in other works on DPD [3,7,8].

To test the validity and limitations of our approach, we also performed a series of focused experiments using a parallel-plate viscometer to measure the viscosity of suspensions of alumina, clay, and talc particles in a sucrose solution at different shear rates. These measurements are used as a comparison for the numerical scheme presented here.

As can be seen, modeling the rheology of these suspensions in a predictable manner involves the consideration of a number of disparate subjects. In this paper, we describe each of these subtopics to the necessary level of detail, along with appropriate references, in order to focus on the main goal of developing a multiscale strategy for real-life applications. We start with a brief description of the materials and the experiments. Then, handling of hydrodynamic and nonhydrodynamic interactions is discussed. This is followed by a brief discussion of some numerical aspects of the multiscale strategy. Finally, comparison between the experiments and numerical results are presented with analysis.

II. MATERIALS AND EXPERIMENTS

This section describes the experimental procedure which was used to obtain the data computed from the numerical model.

A. Material preparation

A 65% (by weight) sucrose solution in water was used as the solvent for the suspensions. The reasons for doing so were multifold: (1) this solution is Newtonian and has a high viscosity of around 175 cP. Thus, it comes close to representing the highly viscous nature of typical solvents used in the extrusion of ceramic pastes. At the same time, its Newtonian nature makes the suspension much simpler to study. (2) Sucrose is a well-studied material and therefore the calculation of interparticle interactions for numerical modeling is straightforward. (3) Sucrose is widely (and cheaply) available. The sucrose used was S6-500 from Fisher Scientific. Making 65% (by weight) sucrose solution in water was straightforward as sucrose dissolves readily in water. The solution preparation process consisted of measuring appropriate amounts of sucrose and water at room temperature and mixing them. The solution was then vibrated for a minute using a vibrator ("Maxi Mix Plus" from Thermolyne) and then kept for a few hours in a slow roller (from US Stoneware, table-top model) to ensure complete dissolution. The roller speed was maintained at 30 rpm. The resulting solution was transparent with a density of 1.3 g/cc and a Newtonian viscosity of around 175 cP.

Three suspensions were made out of finely cut clay, alumina, and talc particles whose particle sizes were controlled to make the suspension size distributions as close to monodisperse as possible. Because of the high viscosity of the solvent and strong interactions between the solvents and the ceramic powders, suspensions were made using a three-roll mill using three to four passes. The solid powders were added to 10 mL of the solvent in 3 g increments until the desired concentration of 30% (by volume) was attained. In practice, the maximum concentration was determined by the ability to blend the suspensions properly using the three-roll mill. The actual solid loading value was obtained from the weight differential between the native suspension and solid part of the suspension after the solvent had been evaporated. In Table I, the suspension and particle properties are listed that are used in the numerical calculations.

TABLE I. Particle and suspension properties.

Solid	Average particle diameter (μm)	Particle density (g/cc)	Loading (% vol)
Clay	2	2	25%
Alumina	1.2	3.5	18%
Talc	2.5	2.5	25%

B. Viscosity measurement

A parallel-plate viscometer (MCR-300 from Anton-Paar Physica) with 50 mm diameter plates and a gap between the plates of 1 mm was used for measuring viscosity. The shear rate was varied from 1 to 1000 s^{-1}. The reading of the normal force between the plates was monitored to ensure the integrity of the measurements. A drawback of parallel-plate viscometer is the centrifugal spilling of the material at high shear rates because of the absence of radial confinement. In view of this, only data for shear rates below 100 s^{-1} were considered reliable, although higher shear rate data did not significantly deviate from the general trend. The measurements were done for both fresh and aged (few days old) suspensions; aging did not have any effect as shown in Fig. 1 for alumina and clay suspensions.

III. RESOLVING THE HYDRODYNAMICS OF THE SOLVENT PHASE

A. Thermostat

In sheared suspensions that have a viscous liquid as the solvent, hydrodynamic effects become critical for the bulk rheology [1–4,6]. Because of its viscous nature, the solvent

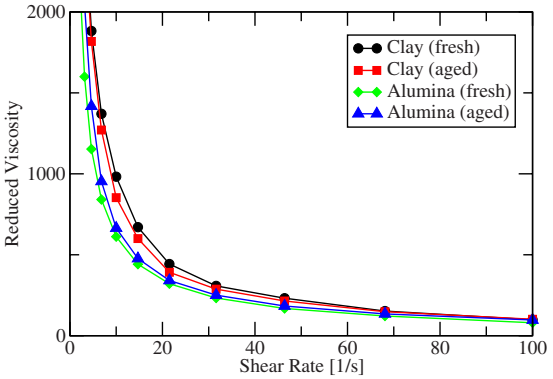

FIG. 1. (Color online) Measured viscosities of fresh and aged sucrose suspensions.

phase acts as an efficient carrier of momentum. Assuming a Newtonian solvent (which is the case in this paper), one of the main objectives of the mesoscopic model is to capture this momentum-carrying capacity as much as necessary [1]. This is because the objective of the exercise is to calculate the rheology of the suspension and not the solvent. Therefore, accurately resolving the viscosity of the solvent is a needless and, as will be seen later, a hopeless task.

The momentum-carrying capacity of a viscous liquid is best captured by the Schmidt number (Sc), which is the ratio of kinematic viscosity to self-diffusivity, ν/D. In essence, Sc quantifies the relationship between the diffusivities of momentum and mass. Liquids are efficient carriers of momentum and hence their Sc values are much greater than 1. The numerical scheme used to resolve the solvent should therefore mimic "liquidlike" Sc numbers, which is of the order of 10 and higher.

One of the drawbacks of the original DPD thermostat with the dissipative and random forces coupled via the fluctuation-dissipation theorem is that it can mimic only low Schmidt numbers ($\sim$1) [9]. Limited success in enhancing Sc can be achieved but at the tremendous cost of extra computations [10]. While this limitation poses no apparent problems for nondilute suspensions with waterlike solvents [2–4], for the system at hand with sucrose solution—almost 200 times more viscous than water—our experience shows that the original DPD thermostat could not resolve the high levels of viscous dissipation.

In view of this, we implemented the Lowe-Andersen (LA) thermostat [7] which can yield Sc numbers orders of magnitude higher than the original DPD implementation. In this thermostat, the coupled dissipative and random forces do not appear explicitly as in the original DPD. Instead, the relative velocity between interaction pairs is frequently and randomly reset using a Maxwell-velocity distribution. The strategy behind enhancing Sc number is to generate additional viscosity (or stresses) from these interactions with the thermostat in a Gallilean-invariant manner. The quantity of these additional stresses can be controlled by thermostat parameters such as the interaction probability, time-step value, etc. [7,8] and thereby Sc of the modeled solvent can be controlled. It should be noted that Gallilean invariance is necessary to conserve hydrodynamics and to render Navier-Stokes representation at macroscopic scales. The LA thermostat does a much better job at this and provides affordable scalability, i.e., computational parameters can be tuned to increase the value of Sc without incurring substantial additional costs [7,8]. Stochastic rotation dynamics (SRD) is another mesoscopic technique in this category that uses a different type of Gallilean-invariant thermostat [1,11].

Finally, a small note is in order before concluding this section. While Schmidt number is an intrinsic fluid property, in this work, we are dealing with mesoscopic scales and so the fluid is described by particles that are much larger than the molecular scale. Therefore, one could easily see that the intrinsic Sc from the molecular description of a fluid may not be exactly the same as Sc from a mesoscopic fluid. Hence, as mentioned above, it is not our goal to "exactly" mimic the solvent Sc in the mesoscopic description [8]. As long as the numerical model can efficiently incorporate the momentum-carrying role of the solvent and resolve the viscous dissipation, the hydrodynamic contribution of the solvent can be accurately accounted for. This fact is important because mimicking high Sc involves high computational costs.

B. Time and length scales analysis

As is well known, a broad spectrum of length and time scales exists in these problems spanning over 10 orders of magnitude. Resolving all of these is impossible [1]. Fortunately, not all of them are important to the bulk rheology of the suspension and hence the spectrum can be "telescoped" to a few scales of relevance [1]. This essentially means mapping the real system into the modeled coarse-grained (CG) system and retaining only the amount of information necessary to meet the objective of describing the rheology of the suspension.

In the systems we are studying that are composed of μm-sized solid particles dispersed in a viscous solvent with imposed shearing, the Peclet number (Pe) is generally much greater than 1 (as mentioned in Sec. VI) and the hydrodynamic effects are dominant over Brownian and colloidal effects. In this rheophysical domain, Pe becomes the most important parameter [12]. The two time scales of importance, therefore, are the diffusive and Stokes time scales. The diffusive time scale (τ_D) is the measure of time it takes a colloid particle to diffuse over a distance of its radius. If "a" is the radius of the colloid then $\tau_D = a^2/D_{coll}$, where the D_{coll} is the diffusivity of the colloid particle in the viscous solvent. Following Einstein's rule, $D_{coll} \sim k_B T/(6\pi\mu a)$, where k_B is Boltzmann's constant, T is the temperature, and μ is the solvent viscosity.

The Stokes time scale (t_s) is the amount of time it takes the colloid particle to advect over a distance equal to its radius and therefore $t_s = a/v$, v being the typical convective velocity in the system. The ratio of τ_D to t_s is the Peclet number and hence it is also the measure of the separation of the relevant time scales, τ_D and t_s. Considering the importance of these two time scales, this separation should be maintained in the modeled, coarse-grained system. Therefore, the physical Peclet number is equated to the Peclet number of the coarse-grained system to ascertain the relevant coarse-grained properties. This is demonstrated by an example below.

Using the expressions of τ_D and t_s, the Peclet number takes the expression $\mathrm{Pe} = 6\pi\mu a^3\gamma/k_B T$, where γ is the imposed shear rate. For a typical case of $\gamma = 10\ \mathrm{s}^{-1}$ and $a = 1\ \mu$m in our sucrose suspension (viscosity of 175 cP) at $T = 300$ K, the physical Peclet number, Pe_r, is 8242. In the coarse-grained system, if the nondimensional scales are so chosen that the nondimensionalized colloid radius is 2 and nondimensionalized $k_B T$ is 1, then the Peclet number of the coarse-grained system takes the form $\mathrm{Pe} = A_0\mu_m\gamma_m$, where μ_m and γ_m are the solvent viscosity and shear rate of the modeled system, respectively, and A_0 incorporates other terms in the Peclet number expression ($6\pi a^3/k_B T$). Equating this with Pe_r yields the relationship between the two quantities as

$$\mu_m\gamma_m = \frac{\mathrm{Pe}_r}{A_0}. \tag{1}$$

Thus, as long as μ_m and γ_m satisfy the above relationship, separation of scales between τ_D and t_s is maintained by the

coarse-grained system and the relevant physics in this rheophysical domain would be captured. But, in practice, not all values of these parameters yield computationally amenable systems and some reasonable bounds must be imposed. For instance, too high a value of γ_m for a chosen system can lead to numerical problems. Also, the choice of these parameters should reasonably maintain the separation of other relevant time scales. The kinematic time scale $\tau_\nu = a^2/\nu$ is the measure of diffusivity of momentum in the solvent phase. Viscous liquids are adept at diffusing momentum much more efficiently than dispersed particles and therefore $\tau_D/\tau_\nu \gg 1$ in a suspension of highly viscous liquid. This disparity should be maintained, if not exactly reproduced, by the choice of the coarse-grained parameters such as μ_m and γ_m [1].

IV. RESOLVING THE NONHYDRODYNAMIC INTERACTIONS

A. Atomistic calculations of solid-solid interactions in sucrose

Although the coarse-grained nature of the mesoscale model places a limit on the accuracy of the interaction potentials, several techniques have been developed (matching forces from atomistic simulations [13], matching experimental potentials [14] or correlation functions [15], and inverting pair-correlation functions [16]) to apply chemical (material) specificity to mesoscale models. A major drawback in developing coarse-grained potentials is the fact that, unlike atomistic potentials, they are sensitive to changes in the system parameters. Simulating a different phase, solvent, or even temperature can require refitting the coarse-grained potentials. However, defining a general approach for one system goes a long way towards reducing the time required to develop potentials for similar systems. In this case, our goal is to develop interaction potentials for colloid suspensions in viscous solvents. Specifically, to demonstrate the procedure, we focus on alumina particles in concentrated sucrose solutions in this section and suggest that potentials for other systems (clay and talc) can be developed using this approach.

Applying the principles of the DPD technique to suspensions in sucrose solutions requires addressing the impact of sucrose on multiple length scales. Not only does it increase the viscosity of the bulk solvent, but it also reduces the electrostatic screening and disrupts the ordering of water molecules near the surfaces of the colloidal particles. The approach used must define the interaction between alumina particles while addressing all of these influences. To accomplish this, we use DLVO theory [5] to the extent that it is applicable to describe the long-range interaction between two flat surfaces and use atomistic simulations to determine the short-range interactions between the surfaces. We then apply the Derjaguin approximation to relate the total interaction between two flat surfaces to the interaction between spheres of the same composition.

DLVO theory accounts for both the van der Waals and double layer interactions between charged surfaces interacting over nanometer to micrometer length scales. The force per unit area due to the double layer term of DLVO theory is shown in Eq. (2) [5]

$$F/A = k_B T \rho_\infty \{[\exp(-e\psi_m/k_B T) - 1] + [\exp(e\psi_m/k_B T) - 1]\}, \tag{2}$$

where k_B is Boltzmann's constant, T is the temperature, ρ_∞ is the bulk ionic strength of the solvent, e is the electronic charge, and Ψ_m is the electrostatic potential at the midplane between the two surfaces. The midplane potential can be written as the sum of the potentials of the two surfaces at the midplane $D/2$, where D is the separation distance between the surfaces

$$\psi_m = (8k_B T \gamma_1/e)\exp(-\kappa D/2). \tag{3}$$

Here, κ is the inverse Debye screening length (using the dielectric constant of a 65% sucrose solution, $\varepsilon = 59.59$ [17]) and γ_1 is given by

$$\gamma_1 = \tanh(ze\psi_0/4k_B T), \tag{4}$$

where z is the valency of the electrolyte ions and ψ_0 is the electrostatic potential on the surface of the alumina particles accounting for the bare surface charge as well as the charge due to the bound ions in the Stern layer. We use a value of 264 mV for the electrostatic potential based on a zeta potential of 97 mV. Using the Derjaguin approximation, the force per unit area from the van der Waals term is given in Eq. (5),

$$F/A = -A_H/6\pi D^3, \tag{5}$$

where A_H is the Hamaker constant and D is the separation distance between the surfaces. The Hamaker constant accounts for the chemical (material) specificity of each surface as well as the properties of the medium between the surfaces. Calculation of the Hamaker constant between different particles is explained in the next section on solid-fluid interaction.

Below a few nanometers, DLVO theory breaks down as the molecular structure of the solvent becomes relevant or as the counter-ion clouds around the particles begin to significantly influence each other. Here, we use targeted molecular dynamics of two alumina surfaces being pushed together to get the solvation potential. In this model, we use the 41213-ICSD structure of bulk alumina taken from the crystal structure database and form the surfaces by cleaving the bulk structure. We then add hydrogen atoms to the exposed oxygen sites at a surface coverage of 1.7 sites/nm^2 corresponding to the measurements of Nordin *et al.* [18]. A 65 wt % sucrose solution is generated from 743 molecules of sucrose in water and equilibrated using the consistent valence force field (cvff). The two alumina surfaces measuring $58 \times 67 \times 12$ Å are put in a simulation box initially separated by 15 Å and solvated with the sucrose solution. The system dimensions are $88 \times 97 \times 69$ Å to provide 30 Å of water between periodic images of the particles. The total number of atoms in the simulation is 38 852. The targeted MD approach involves gradually pushing the two surfaces together while measuring the force experienced by the surfaces. The interactions between the individual atoms are described by the ClayFF force field [19] and parameters for the sucrose molecules are taken from the cvff force field [20,21]. The simulations are performed in the NVE ensemble using a time step of 0.4 fs with temperature rescaling applied every ten steps

to maintain the temperature at 300 K. The surfaces are incrementally pushed together by a distance of 0.5 Å over a time of 40 ps followed by 360 ps of data collection to determine the average force on the surfaces at each stage. Using this approach, the short-range interactions due to solvation forces, which are not taken into account by DLVO theory, can be accurately calculated and added to the DLVO forces. At the end of the simulation, the solvation potential is calculated by integrating the force on each surface at each separation distance relative to the system at infinite separation.

$$E_{solv}(D) = -\int_{\infty}^{D} F(r)dr. \tag{6}$$

Whereas solvation potentials often show an oscillatory profile when the solvent is pure water, the presence of sucrose disrupts the water structure near the particle surfaces and we get a solvation potential that shows a smooth exponential decay. Similarly, the two components of the DLVO potential can be fit to exponential functions that are practical for incorporating into coarse-grained simulations. This gives us a set of CG force field parameters that account for the surface chemistry and charge density of alumina surfaces in sucrose solutions.

After calculating the solvation and DLVO forces between the solid surfaces, the net solid-solid interaction potential per unit area at a distance D between the surfaces can be generalized as shown in Eq. (7) for use in the DPD simulations. Although the components of the potential are determined numerically, we find that this expression gives a near-perfect fit to the numerical results

$$E_{surf}(D)/A = \left(A_1 \exp(-B_1 D) + A_2 \exp(-B_2 D) + C_2 - \frac{A_H}{12\pi D^2}\right). \tag{7}$$

Here, the terms with subscript 1 pertain to the ultraclose range solvation potential obtained by fitting the numerical results of MD simulations. The terms with subscript 2 pertain to the electrostatic component of the DLVO potential and are obtained by numerically integrating Eq. (2). The last term is the attractive van der Waals component of the DLVO potential which can be obtained by analytically integrating Eq. (5). These terms bring material specificity to the rheology of the suspension in an analytical form that is efficient to calculate and easy to incorporate into the DPD simulations. The values of these parameters for different solid materials are listed in Sec. VI on numerical simulations. The interaction energy per unit area obtained by combining the solvation and DLVO components for two alumina surfaces in a sucrose suspension is shown in Fig. 2. With this expression, the force between two alumina spheres can be written as $F_{\text{sphere}}(D) = \pi R E_{surf}(D)/A$ using the Derjaguin approximation where the factor of πR accounts for the curvature of the spherical particle surfaces. Specifically, R is the geometric mean of the radii of the two particles.

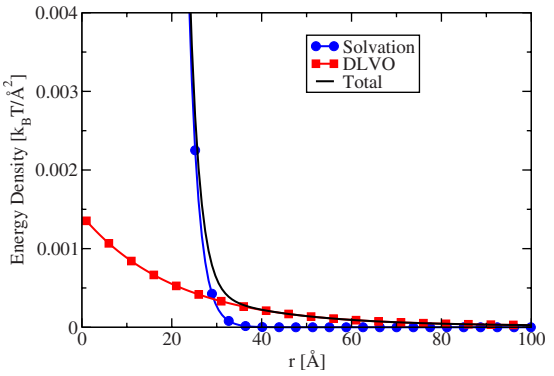

FIG. 2. (Color online) Form of the interaction energy per unit area between two alumina surfaces in a sucrose solution.

B. Solid-fluid particle interactions

Although the interaction between two colloidal particles is well described by theory and can be measured experimentally, the interaction between a colloid and a mesoscopic fluid particle is poorly defined. The reason for this is the fluid particle is intended to represent many fluid molecules that, unlike the atoms comprising the colloidal particle, are not bound together. In this work, a LJ potential is used to describe the interaction between the fluid and solid particles. The motivation behind its use comes from its proven versatility and its widespread use in many applications including mesoscopic systems as in Refs. [22,23]. This potential is defined as

$$E_{\text{sl}}(r) = 4\varepsilon_{\text{sl}}\left\{\left(\frac{\sigma_{\text{sl}}}{r}\right)^6 - \left(\frac{\sigma_{\text{sl}}}{r}\right)^{12}\right\}. \tag{8}$$

Since this is an interaction between two mesoscopic particles, the LJ parameters ε_{sl} and σ_{sl} in this context need a mesoscopic interpretation and they should pertain to the size and the materials of the interacting particles. Since the solid particles are larger than the fluid particles, σ_{sl} is the measure of the repulsive core of the solid particle and therefore is taken to be of the order of the radius of the solid particle (typically 1.1 to 1.2 times the radius). Larger values of σ_{sl} lead to less affinity between the solid particle and the solvent. For a mesoscopic interpretation of the well depth, ε_{sl}, the following approach is used.

As shown by Everaers and Ejtehadi [24], for two homogeneous particles, integrating the atomistic LJ potential over the volumes of the particles allows one to relate the mesoscopic Hamaker constant (A_H) to the atomistic LJ parameters, $A_H = 4\pi^2 \varepsilon_{\text{LJ}} (\rho\sigma^3)^2$. Generalizing to the case of heterogeneous particles where the first particle is composed of type-i components and the second particle is composed of type-j components, we can write the following expression for A_H if we assume that the density of each component is distributed evenly throughout the particles:

$$A_H = 4\pi^2 \rho_1 \rho_2 \sum_{i,j} x_i x_j \varepsilon_{ij} \sigma_{ij}^6, \tag{9}$$

where x_i is the mole fraction of atom type i in particle 1 and x_j is the mole fraction of atom type j in particle 2.

TABLE II. Effective mesoscopic interaction parameters for the alumina and sucrose particles.

Pair type	A_H (k_BT)
Alumina-alumina	57.6
Alumina-sucrose	41.4

After tabulating the mole fractions of each atom type in our solvent and alumina particles, we obtain the Hamaker constants for particles of alumina and 65% sucrose solution shown in Table II. For the case of the solid-fluid interaction between alumina and sucrose (fluid) particles, the Hamaker constant is interpreted as ε_{sl} in the LJ interaction, Eq. (8). The Hamaker constants for clay and talc suspensions are calculated using a similar procedure and are given in Sec. VI where simulation results are presented.

We include here a potential accounting for the particle-solvent interaction, yet above, we derive the effective particle-particle interactions while including the solvation forces due to an explicit solvent. We use this approach because the solvent particles in our DPD simulations are half the size of the alumina particles. Although the solvent particles are soft particles, they are much larger than the interaction range of the solvation forces, which is less than 10 nm. When the alumina particles are close enough together in the DPD simulation for solvation forces to become relevant, there are no fluid particles between them. Here, the solvation potential derived from atomistic simulation is used to describe the repulsive interaction between the alumina particles.

V. NUMERICAL CONSIDERATIONS

There are many numerical issues associated with simulating a system as complex as the one at hand. The presence of a broad spectrum of length and time scales, the necessity to resolve high Schmidt numbers, and the inherently expensive nature of particle-based computational techniques are but a few of the complexities associated with these systems. Below is a brief account of some numerical details that were found to be important.

A. Solvent thermostat

As mentioned previously, it was found necessary to use the Lowe-Andersen thermostat since it can resolve high Schmidt numbers. Using this thermostat, an interaction pair is thermalized with a probability that is proportional to the Schmidt number of the modeled solvent. Within a certain bound, Sc increases as the probability increases, but the computational expense is also higher due to the larger number of velocity readjustment operations involved. For our systems, it was found that no substantial benefit was achieved above a probability of 0.3. This is due to the small value of the time step (as discussed below) that ensures a large number of interactions with the thermostat bath [7].

B. Initiating shear in dense suspensions

Because of the presence of strong attractive components in the solid-solid and solid-solvent interactions, the viscosities are very high at low shear rates where colloidal interactions dominate and the suspension appears to be essentially in a jammed state. (This is also observed experimentally.) Accordingly, special attention needs to be paid to the simulations at the initial stages to get the system into computationally amenable configurations where hydrodynamic effects start becoming important. Otherwise, it was seen that the energies in the simulations tend to diverge very soon.

This was accomplished by beginning the simulations with values of the LJ ε parameter [Eq. (8)] 5 orders of magnitude less than the actual value and increasing it linearly to the actual value over the first 100 000 time steps. The total duration of the simulations is long enough (of the order of 15–20 million time steps) to negate the effect of this artifice. Besides, time averaging of stress and velocities is typically done after the first 2 000 000 time steps thus eliminating any possibility of any lingering effect of this operation. Physically, this numerical artifice implies that initially and for a very short duration, the suspension is made less "sticky" so that the particles get some maneuvering room to move out of jammed (or near-jammed) configurations without requiring additional measures to resolve the stress fluctuations that are present in this regime [25,26].

C. Reduced units

A standard nondimensionalization procedure [3,4] is used in which the nondimensionalization parameters are the cutoff radius r_c for length, mass of the DPD fluid particle for mass, and k_BT for energy. Dimensionless values of hydrodynamic parameters such as shear rate and solvent viscosity, however, are calculated using the analysis presented in Sec. III B.

The value of nondimensional colloid radius (the ratio of the radius of the solid particle to the cutoff radius) has important implications as it determines the hydrodynamic length scales being resolved (or ignored). The larger the value of this radius, the smaller the length scales resolved, but then one needs larger domain size, which results in more computations. Following the detailed analysis presented in Ref. [1], in this work we used a value of 2 for nondimensional colloid radius.

D. Simulation time step

Time scales associated with nonhydrodynamic interactions (solid-solid and solid-solvent) are much smaller than the ones associated with hydrodynamic phenomena [1]. Therefore, the value of the simulation time step depends on the steepness of the electrostatic interactions (solid-solid and solid-liquid). For the cases considered here, a simple analysis of the solid-solid and solid-solvent interactions for some typical parameters indicate that the solid-solid interactions are the most demanding and hence the simulation time step is based on effectively resolving them. In order to arrive at a conservative estimate, the interaction force at a very small surface separation (0.001 in dimensionless units) is used. To

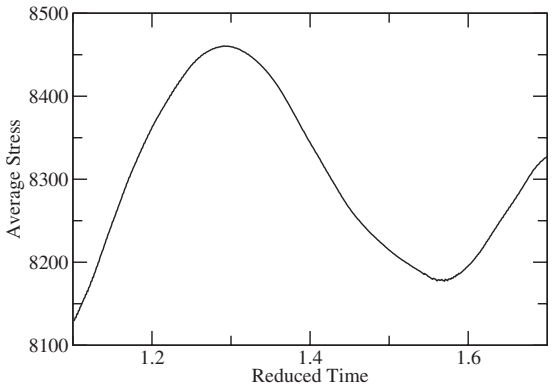

FIG. 3. An example of the temporal variation of stress with time for the alumina suspension at a shear rate of 10 s^{-1}. The average amplitude of the oscillations gives a minimum estimate for the error in the reported results.

estimate the simulation time step, we require that under the interaction forces at this separation, the particle should not move more than $0.1r_c$ during one time step. Note that analysis of this kind only gives a rough estimate of the order of magnitude of the time step. The appropriate value depends on the physical nature of the problem and often some trial and error as well as intuition. For the suspensions considered here, dimensionless time steps were in the range of 10^{-8}–10^{-7}.

E. Duration of the simulation

In these simulations, macroscopic quantities such as viscosity are calculated using small time-step values chosen to resolve the nonhydrodynamic interactions that are much smaller than the time scales associated with hydrodynamic phenomena. Hence, long simulations are needed to obtain statistically homogeneous solutions. This is also the case because in time-discrete numerical simulations, small time steps result in very slow changes in the value of the stresses, which can be temptingly misconstrued as a converged solution. Our experience has shown that the number of time steps needed to assure a converged stress value is in excess of 15 million. The signs of convergence are either an almost constant value over 2–3 million time steps or oscillations around an average value. In the latter case, the amplitude of the fluctuations gives a minimum estimate of the error. Our simulations were extended until the errors due to the oscillations in the averaged stress were less than 5%. In Fig. 3, we show a typical averaged stress profile near the end of the simulation of the alumina suspension. As can be seen, the variation is roughly 3% of the averaged stress.

VI. NUMERICAL SIMULATIONS AND ANALYSIS

With the philosophy and formulation described above, numerical simulations were carried out on suspensions of alumina, clay, and talc particles with the intention of validating the formulation by comparing to experimental data. For each simulation, a domain size of $16\times16\times16$ (in dimensionless units) was used. Since these simulations involve computational particles of different sizes (solid particles being larger than fluid particles), a size-dependent neighbor search algorithm was implemented [27]. In this algorithm, direct-find and linked-list search algorithms were applied separately to the particle pairs. A linked-list algorithm is much faster but to make it work for disparate particle sizes involves quite some work [27]. Direct find, on the other hand, is a simpler method that can be applied to disparate particle sizes but is computationally expensive. A hybrid scheme was implemented that harnesses the advantages of each of these schemes and provides a 4–5 times decrease in computational time over just the direct-find method. All fluid-fluid pairs that involve same-sized particles (which far outnumber fluid-solid and solid-solid pairs) were probed using the faster linked-list algorithm. The other pair types were probed using the direct-find method. The Lees-Edwards boundary condition was used to numerically impose the shear rate [27].

For solid particles, a spherical, monodisperse distribution with particle size equal to the measured averaged particle diameter is used for all the simulations. This is an approximation since despite our best efforts, some polydispersity in particle size does exist. The viscosity of the suspension is obtained by dividing the calculated stress by the imposed shear rate. The stress has three main components: (1) all valid interactions between the constituent particles (solid-solid, solid-solvent, and solvent-solvent interactions), (2) the kinetic contribution term due to the motion of the particles (mv_iv_j, v_i, and v_j are the velocity components relative to the reference frame), and (3) the extra collisional term due to the interaction of the particles with the LA thermostat [7]. All these components are averaged over volume and time to arrive at the stress [27]. The validation of the basic numerical formulation and application to simpler problems has been reported by Chatterjee in Refs. [4,10].

TABLE III. Interaction parameters for the alumina suspension as defined in Eq. (7). These parameters are obtained by fitting atomistic MD simulation results or numerical integration as detailed in Sec. IV. To improve the accuracy of the fit, two values have been fitted to parameters with subscript 2 depending on the separation distance, D, between the particles.

Parameter	Value	Units
A_H	57.6	k_BT
A_1	169.988	$k_BT/\text{Å}^2$
B_1	0.446	$1/\text{Å}$
	$D<100$ Å	
A_2	0.001404	$k_BT/\text{Å}^2$
B_2	0.048169	$1/\text{Å}$
C_2	1.58×10^{-5}	$k_BT/\text{Å}^2$
	$D>100$ Å	
A_2	0.00035	$k_BT/\text{Å}^2$
B_2	0.025867	$1/\text{Å}$
C_2	0	$k_BT/\text{Å}^2$

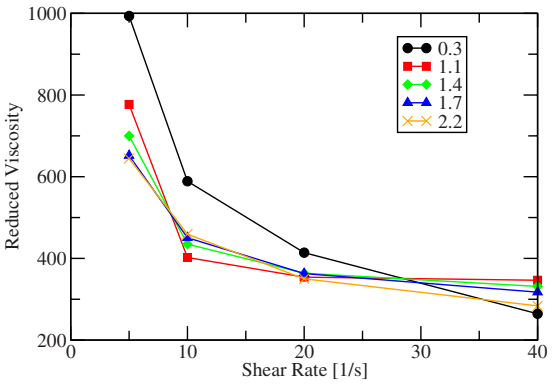

FIG. 4. (Color online) Numerically calculated viscosities of the 18% alumina suspension after simulations for indicated reduced times (time step=10^{-7}).

A. Alumina suspension

For the 18% alumina suspension whose properties are listed in Table I, the calculated parameters for the solid-solid interactions, Eqs. (7) and (8) are given in Table III. The cutoff radius used for this system is 0.3 μm (half the colloid radius). The Lennard-Jones parameters for the solid-liquid interaction are ε_{sl}=41.4 k_BT and σ_{sl}=0.66 μm (1.1 times the colloid radius). The solvent viscosity is set to μ_m=10. The Peclet number varies from 865 to 6920 as we vary the shear rate from 5 to 40 s^{-1}. As mentioned above, such high values of Pe indicate that hydrodynamic effects dominate over colloidal effects in the rheophysical domain considered. We simulated 22 million time steps (reduced time of 2.2) to attain convergent values for the viscosities as shown in Fig. 4. For this suspension, the total strain reached at the lowest Pe simulated (865) was 1.26 (for a time-step value of 10^{-7} and total number of time steps of 22 million). In Fig. 5, the calculated reduced viscosities are compared to experimental data. In Fig. 6, the same is plotted on a log-log scale for clarity. The comparison is good at higher shear rates and it deteriorates at lower shear rates where experimental values rise far more steeply than the numerical results. An analysis of this observation will be presented at the end of this section.

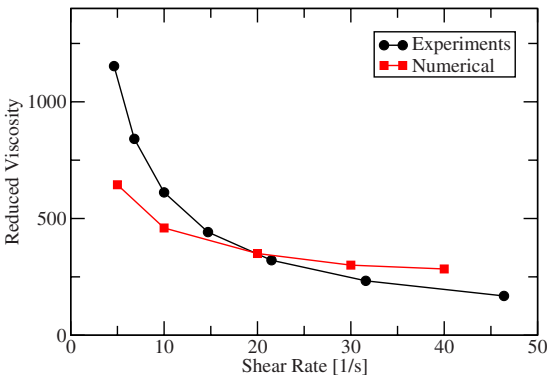

FIG. 5. (Color online) Comparison of viscosities from experiment and numerical simulation of an 18% alumina suspension.

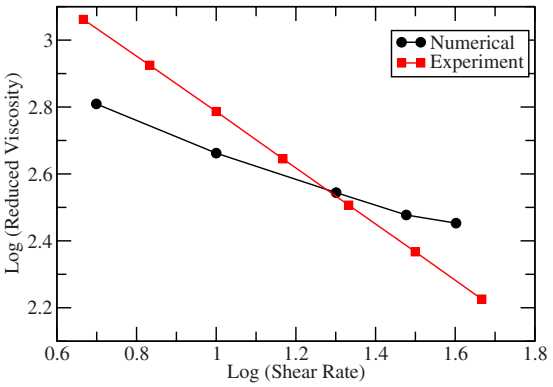

FIG. 6. (Color online) Fig. 5 on a log-log scale.

B. Clay suspension

Properties of the clay particles and 25% clay suspensions are given in Table I. The Peclet number varies from 1600 to 24 000 in the shear rate range of 2–30 s^{-1}. The cutoff radius used for this system is 0.5 μm. Here, the solvent viscosity is set to μ_m=50 and the Lennard-Jones parameters for the solid-liquid interaction are ε_{sl}=45.4 k_BT and σ_{sl}=1.2 μm. The parameters for the solid-solid interactions are listed in Table IV. The total strain reached for the lowest Pe was 1.06 (time step=10^{-7} and total number of time steps of 50 million).

The calculated reduced viscosities are compared to the experimental data in Fig. 7 and a log-log plot is shown in Fig. 8. As in the alumina case, the values compare very well at higher shear rates, while at lower shear rates, the experiments show higher viscosity values. Both for clay and alumina, a shear-thinning behavior is observed in both the numerical simulations and the experiments, as expected.

TABLE IV. Interaction parameters for the clay suspension as defined in Eq. (7). These parameters are obtained by fitting atomistic MD simulation results or numerical integration as detailed in Sec. IV. To improve the accuracy of the fit, two values have been fitted to parameters with subscript 2 depending on the separation distance, D, between the particles.

Parameter	Value	Units
A_H	69.3	k_BT
A_1	25.068	$k_BT/\text{Å}^2$
B_1	0.1193	$1/\text{Å}$
	$D<100$ Å	
A_2	0.002773	$k_BT/\text{Å}^2$
B_2	0.0259	$1/\text{Å}$
C_2	8.43×10^{-5}	$k_BT/\text{Å}^2$
	$D>100$ Å	
A_2	0.001697	$k_BT/\text{Å}^2$
B_2	0.017	$1/\text{Å}$
C_2	0	$k_BT/\text{Å}^2$

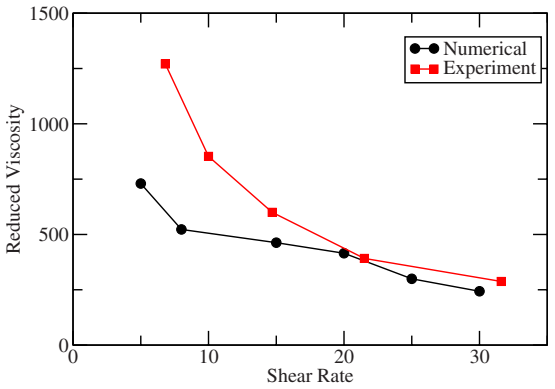

FIG. 7. (Color online) Comparison of viscosities from experiment and numerical simulation of a 25% clay suspension.

C. Talc suspension

Properties of the talc particles and 25% talc suspensions are given in Table I. Among the three, talc particles are the largest in size and hence the suspensions have a much higher Peclet number that varies from 3940 to 59 100 in the shear rate range of 2–30 s^{-1}. The cutoff radius used for this system is 0.625 μm. Here, the solvent viscosity is set to $\mu_m = 50$ and the Lennard-Jones parameters for the solid-liquid interaction are $\varepsilon_{sl}=41.9\ k_BT$ and $\sigma_{sl}=1.5\ \mu$m. The parameters for solid-solid interactions are listed in Table V. The total strain reached for the lowest Pe was 1.3 (time step $=10^{-7}$ and total number of time steps of 50 million).

The calculated reduced viscosities are compared to the experimental data in Fig. 9. A log-log plot is shown in Fig. 10. The same trend seen for the clay and alumina cases above is seen here. Experimentally measured talc suspension viscosities are almost 3 times higher than those for clay (and alumina) suspensions for comparable solid loading of 25%. Of the three suspensions reported, this suspension shows the greatest amount of discrepancy from the experiments, particularly at the lower shear rates ($<10\ s^{-1}$).

D. Analysis

Simulations of the three suspensions show reasonable agreement with experiments at higher shear rates but fail to capture the steep rise in viscosity as the shear rate is reduced below 10 s^{-1}. The values, though, are of the same order of magnitude as seen in Figs. 5, 7, and 9. From the log-log plots, Figs. 6, 8, and 10, it can be seen that more or less for all the three cases, the experiments show a dependence of viscosity on shear rate as $\mu \sim (\gamma)^{-1}$, whereas for the numerical calculation, the exponent has a value close to $-1/2$, quite consistently across the board. Of the three, calculations for alumina suspension are closest to the experimental data and talc suspension shows the most discrepancy. This is understandable considering the fact that alumina suspension has the least solid loading (18%) and smallest particle size and talc suspension has the largest particle size and highest solid loading (25%). As the particle sizes and loading fractions get lowered, the particle shape becomes less important. One obvious reason for the discrepancies seen in all of these cases is the simplified spherical, monodisperse particles used in the simulations. In reality, particles are polydisperse and aspherical. It is known that particle shape can affect suspension

TABLE V. Interaction parameters for the talc suspension as defined in Eq. (7). These parameters are obtained by fitting atomistic MD simulation results or numerical integration as detailed in Sec. IV. To improve the accuracy of the fit, two values have been fitted to parameters with subscript 2 depending on the separation distance, D, between the particles.

Parameter	Value	Units
A_H	58.9	k_BT
A_1	37.08	$k_BT/\text{Å}^2$
B_1	0.201	$1/\text{Å}$
	$D<100$ Å	
A_2	0.008182	$k_BT/\text{Å}^2$
B_2	0.03255	$1/\text{Å}$
C_2	2.073×10^{-5}	$k_BT/\text{Å}^2$
	$D>100$ Å	
A_2	0.00239	$k_BT/\text{Å}^2$
B_2	0.01588	$1/\text{Å}$
C_2	0	$k_BT/\text{Å}^2$

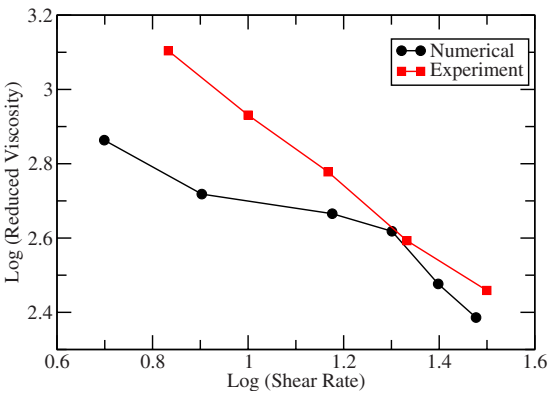

FIG. 8. (Color online) Log-log plot of Fig. 7.

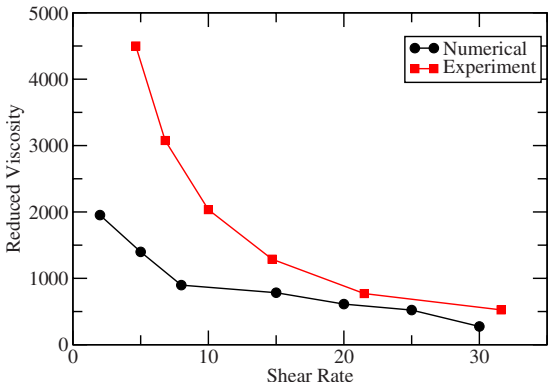

FIG. 9. (Color online) Comparison of viscosities from experiments and numerical simulations of a 25% talc suspension.

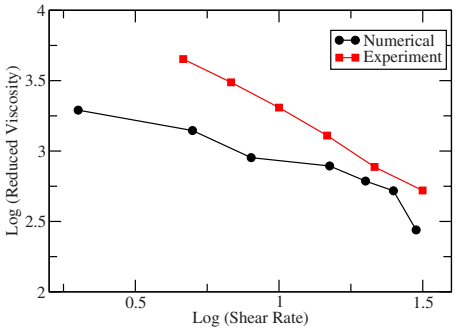

FIG. 10. (Color online) Log-log plot of Fig. 9.

viscosity, more so at the lower ends of the hydrodynamic regime [4].

Another reason may be the inherent limitation associated with measuring the viscosity of particulate suspensions using a parallel-plate viscometer. As described in Ref. [28], particle migration away from the walls in a sheared suspension gives rise to a segregated microstructure, so that regions near the wall have a lower solid loading than regions away from the walls. As a result, rheological measurements using this technique have local characteristics that need to be taken into account and the net viscosity reported by the viscometer does not exactly pertain to the uniformly dispersed systems the numerical scheme deals with. In fact, the measurement of viscosity of particulate suspensions still remains a challenging task [28].

However, we think that the above reasons are secondary and there are other, deeper, issues involved. As the shear rate increases, the hydrodynamic effects start dominating the colloidal and Brownian interactions and take the system to flow-amenable configurations thereby reducing the viscosity. At low shear rates where the colloidal interactions are more dominant, experiments suggest an almost abrupt rise in viscosity which the numerical simulations fail to capture. This behavior is very similar to the abrupt rheological behavior of dense suspensions near the yielding regime seen experimentally [25,26]. In this regime, these suspensions show an "avalanche"-type behavior wherein the viscosity drops rapidly at the onset of yielding or, looked at in the reverse direction, the viscosity rises rapidly as the system approaches the jammed state and the formulation does not seem to be able to capture this.

A more generic way of looking at yielding of granular paste is the process of unjamming a jammed configuration [29] and there is enough experimental evidence to suggest that this process is accompanied by transient stress fluctuations that are responsible for the steep viscosity behavior in this regime [25,26,30–32]. Our suspensions, although not highly dense from a solid loading point of view, nevertheless behave like one because of the presence of strong attractive potentials, particularly at low shear rates where colloidal interactions are more effective [29,30]. Hence, at low shear rates, in the vicinity of jamming-unjamming transitions, stress fluctuations exist that are not captured by the mesoscopic scheme used here, possibly because of the scaling assumptions. These fluctuations have additional dissipations associated with them that give rise to higher viscosities with a steeper rise as evidenced in our experimental data. We believe that the contributions of these fluctuations to viscous dissipation constitute a big part of the gap between the numerical results and experimental data at low shears.

In order to capture the behavior at low shear rates, a mechanism needs to exist to incorporate the additional stress fluctuations in the present mesoscopic numerical scheme. Prior to that, however, one needs to understand the nature of these fluctuations and try to represent them in a closed-form, accessible manner. Our thesis in this regard is that these fluctuations need not be incorporated accurately at their native scales but rather their effect can be coarse grained as effective dissipative terms. This is akin to the manner in which the effects of turbulent fluctuations are incorporated as an effective Reynolds stress term in Navier-Stokes equation in two-equation models [33]. These issues, in our opinion, lie at the core of understanding the behavior of complex suspensions at low shear rates and are presently being investigated.

VII. CONCLUSIONS

In this paper, a successful attempt was made to predict the rheology of real suspensions, quantitatively, using a multiscale methodology that incorporates the effect of material properties on macroscopic viscosity. Aside from the well-studied factors such as particle shape and size, solid loading, etc., it is well known that material properties have a profound effect on bulk rheology. In this work, we presented a tested methodology to quantitatively account for this material specificity. To do this, we used atomistic MD simulations along with DLVO theory to calculate the solid-solid interaction and we used an LJ-type interaction for the solid-solvent interaction. The parameters of these interactions were calculated using the actual material properties thus bringing material specificity to the scheme. The calculated viscosities compare reasonably well to experimental measurements at the higher end of the shear rate spectrum considered and show discrepancy at lower shear rates, although the values are of the same order of magnitude and show a similar trend. Specifically, the computations are unable to reproduce the steep rise in viscosity as the shear rate goes to zero. Some explanations have been put forward to explain this. We propose that at low shear rates, the transition to jammed configurations is accompanied by stress fluctuations that are not accounted for in the mesoscopic, DPD-type technique used here.

Finally, it should be noted that there are numerous variables involved in the characteristics and experimentation of these suspensions most of which cannot be possibly incorporated in a modeling exercise and hence very close agreement with experiments is almost impossible for these cases. However, by incorporating the essential features and by adopting a first-principles-based multiscale strategy, reasonable agreement was obtained and the trends were reproduced. Also, very high Peclet numbers ($\sim 10^4$) were resolved. Overall, the strategy and analysis presented can be used as a stepping stone to make mesoscopic techniques such as DPD a valuable tool for the prediction of rheology for practical applications.

[1] J. T. Padding and A. A. Louis, Phys. Rev. E **74**, 031402 (2006).
[2] P. J. Hoogerbrugge and J. M. V. A. Koelman, Europhys. Lett. **19**, 155 (1992).
[3] R. G. Groot and P. B. Warren, J. Chem. Phys. **107**, 4423 (1997).
[4] A. Chatterjee and L. M. Wu, Mol. Simul. **34**, 243 (2008).
[5] J. Israelachvili, *Intermolecular and Surface Forces* (Academic Press, New York, 2003).
[6] J. F. Brady and G. Bossis, J. Fluid Mech. **155**, 105 (1985).
[7] C. P. Lowe, Europhys. Lett. **47**, 145 (1999).
[8] E. A. J. F. Peters, Europhys. Lett. **66**, 311 (2004).
[9] C. A. Marsh and J. M. Yeomans, Europhys. Lett. **37**, 511 (1997).
[10] A. Chatterjee, Mol. Simul. **33**, 1233 (2007).
[11] A. Malevanets and R. Kapral, J. Chem. Phys. **110**, 8605 (1999).
[12] P. Coussot and C. Ancey, Phys. Rev. E **59**, 4445 (1999).
[13] S. Izvekov and G. A. Voth, J. Chem. Phys. **123**, 134105 (2005).
[14] A. Lozsán, M. García-Sucre, and G. Urbina-Villalba, Phys. Rev. E **72**, 061405 (2005).
[15] H. Meyer, O. Biermann, R. Faller, D. Reigh, and F. Müller-Plathe, J. Chem. Phys. **113**, 6264 (2000).
[16] P. G. Bolhuis, A. A. Louis, J. P. Hansen, and E. J. Meijer, J. Chem. Phys. **114**, 4296 (2001).
[17] W. M. Arnold, A. G. Gessner, and U. Zimmermann, Biochim. Biophys. Acta **32**, 1157 (1993).
[18] J. Nordin, P. Persson, E. Laiti, and S. Sjoberg, Langmuir **13**, 4085 (1997).
[19] R. T. Cygan, J.-J. Liang, and A. G. Kalinichev, J. Phys. Chem. B **108**, 1255 (2004).
[20] S. Lifson, A. T. Hagler, and P. Dauber, J. Am. Chem. Soc. **101**, 5111 (1979).
[21] P. Dauber-Osguthorpe, V. A. Roberts, D. J. Osguthorpe, J. Wolff, M. Genest, and A. T. Hagler, Proteins: Struct., Funct., Bioinf. **4**, 31 (1988).
[22] V. Pryamitsyn and V. Ganesan, J. Chem. Phys. **122**, 104906 (2005).
[23] W. Dzwinel, D. A. Yuen, and K. Boryczko, J. Mol. Model. **8**, 33 (2002).
[24] R. Everaers and M. R. Ejtehadi, Phys. Rev. E **67**, 041710 (2003).
[25] D. Lootens, H. Van Damme, and P. Hebraud, Phys. Rev. Lett. **90**, 178301 (2003).
[26] P. Coussot, Q. D. Nguyen, H. T. Huynh, and D. Bonn, Phys. Rev. Lett. **88**, 175501 (2002).
[27] M. P. Allen and D. J. Tildesley, *Computer Simulation of Liquids* (Oxford University Press, New York, 1987).
[28] N. Huang and D. Bonn, J. Fluid Mech. **590**, 497 (2007).
[29] A. J. Liu and S. R. Nagel, Nature (London) **396**, 21 (1998).
[30] V. Trappe, V. Prasad, L. Cipelletti, P. N. Segre, and D. A. Weitz, Nature (London) **411**, 772 (2001).
[31] F. Dalton, F. Farrelly, A. Petri, L. Pietronero, L. Pitolli, and G. Pontuale, Phys. Rev. Lett. **95**, 138001 (2005).
[32] D. Lootens, H. van Damme, Y. Hemar, and P. Hebraud, Phys. Rev. Lett. **95**, 268302 (2005).
[33] W. D. McComb, *The Physics of Fluid Turbulence* (Oxford University Press, New York, 1992).